

Al/Ti/Al phonon-mediated KIDs for UV-VIS light detection

**L Cardani¹, N Casali¹, A Cruciani¹, H le Sueur², M Martinez^{3,1},
F Bellini^{3,1}, M Calvo⁴, M G Castellano⁵, I Colantoni⁴, C Cosmelli^{3,1},
A D'Addabbo⁶, S Di Domizio^{7,8}, J Goupy⁴, L Minutolo^{3,1},
A Monfardini⁴, M Vignati¹**

¹INFN - Sezione di Roma, Piazzale Aldo Moro 2, 00185, Roma - Italy

²CSNSM, Univ. Paris-Sud, CNRS/IN2P3, Universit  Paris-Saclay, 91405 Orsay, France

³Dipartimento di Fisica - Sapienza Universit  di Roma, Piazzale Aldo Moro 2, 00185, Roma - Italy

⁴Institut Neel, CNRS/UJF, 25 rue des Martyrs, BP 166, 38042 Grenoble, France

⁵Istituto di Fotonica e Nanotecnologie - CNR, Via Cineto Romano 42, 00156, Roma - Italy

⁶INFN - Laboratori Nazionali del Gran Sasso, Assergi (L'Aquila) I-67010 - Italy

⁷Dipartimento di Fisica - Universit  degli Studi di Genova, Via Dodecaneso 33, 16146, Genova - Italy

⁸INFN - Sezione di Genova, Via Dodecaneso 33, 16146, Genova - Italy

E-mail: angelo.cruciani@roma1.infn.it

Abstract. The development of wide-area cryogenic light detectors with baseline energy resolution lower than 20 eV RMS is essential for next generation bolometric experiments searching for rare interactions. Indeed the simultaneous readout of the light and heat signals will enable background suppression through particle identification.

Because of their excellent intrinsic energy resolution, as well as their well-established reproducibility, Kinetic Inductance Detectors (KIDs) are good candidates for the development of next generation light detectors. The CALDER project is investigating the potential of phonon-mediated KIDs.

The first phase of the project allowed to reach a baseline resolution of 80 eV using a single KID made of aluminium on a 2x2 cm² silicon substrate acting as photon absorber. In this paper we present a new prototype detector implementing a trilayer aluminium-titanium-aluminium KID. Thanks to the superconducting proximity effect the baseline resolution improves down to 26 eV.

1. Introduction

In the last decade, Kinetic Inductance Detectors (KIDs)[1] underwent a rapid development, allowing their successful application to millimeter [2] and UV astronomy [3]. Different projects are currently on-going with the aim to apply this technology to other fields, ranging from the search of extrasolar planets [4] to X-ray spectroscopy [5, 6].

The CALDER project [7] is developing large area phonon-mediated KIDs with the aim of detecting small amounts of ultraviolet-visible (UV-VIS) light. Such detectors will play a crucial role for the next-generation bolometric experiments searching for neutrinoless double- β decay. CUORE [8], the current leading bolometric experiment, is an array of 988 TeO_2 crystals read by NTD sensors. Its sensitivity to double- β decay is mainly limited by the background induced by the α radioactivity of the material surrounding the detector at cryogenic temperature, mainly copper. The possibility to distinguish different particles would allow to overcome this limit. Particle identification could be accomplished by measuring the Cherenkov light (≈ 100 eV) emitted in a TeO_2 crystal by electrons, that are the signal candidates, but not by α particles [9, 10, 11]. CUPID[12, 13], the planned upgrade of CUORE, will therefore require light detectors able to monitor the whole face of a crystal (≈ 25 cm²) with a baseline energy resolution good enough to clearly detect this tiny amount of light (< 20 eV RMS).

One of the limits of KIDs is that they can reach a maximum sensible area of a few mm²[14]. To increase the sensible area to several cm² we opted for a phonon-mediated approach[15]: photons are absorbed by the silicon substrate on which the KID is deposited and produce athermal or ballistic phonons able to reach the KID, where they break Cooper pairs and generate a signal. The use of KIDs as phonon-mediated detectors was firstly proposed for the detection of cosmic rays [15] and X-rays [16, 17]. The application of such detectors to detect visible light was initially studied by the CALDER project, using an array of 4 KIDs [18], made of aluminium and lithographed on a 2×2 cm², 300 μm thick silicon substrate. Recently it was demonstrated a baseline resolution of 82 eV using a single KID made of aluminium[19]. In the following we describe a resolution improvement down to 26 eV, obtained using a trilayer KID made of titanium (Ti) and aluminium (Al).

2. Detector description

KIDs base their working principle on the kinetic inductance of Cooper pairs, which can be modified by an energy release able to break them into quasi-particles (QPs). If the superconductor is inserted in a resonant RLC circuit with high quality factor ($Q > 10^3$), the density variation of QPs modifies the transfer function S_{21} of the resonator both in phase and in amplitude. The phase readout is usually preferred

since the phase response is larger (up to a factor 10) and is given by [18]:

$$\frac{d\phi}{dE} = \eta \frac{\alpha S_\phi(\omega, T) Q}{N_0 V \Delta_0^2} \quad (1)$$

where η is the energy to QPs conversion efficiency, α is the fraction of kinetic inductance with respect to total inductance, Δ_0 is the superconducting gap, N_0 is the single spin density of states and V the detector volume. $S_\phi(\omega, T)$ is a dimensionless factor given by the Mattis-Bardeen theory, describing the phase responsivity as a function of frequency and effective temperature [20]. Finally Q is the quality factor of the resonator. The detector described in [19], made of a 60 nm thick Al film, featured $\eta = 7.4\%$, $\alpha = 2.5\%$, $Q = 1.5 \times 10^5$, $\Delta_0 = 179 \mu\text{eV}$, $V = 2.4 \times 10^5 \mu\text{m}^3$, $S_\phi = 2.85$, while for aluminium $N_0 = 1.72 \times 10^{10} \text{ eV}^{-1} \mu\text{m}^{-3}$.

One way to improve the responsivity is to increase the fraction of kinetic inductance α and to reduce the superconducting gap Δ_0 , without affecting significantly the other parameters in Eq. 1. This can be achieved by exploiting the superconducting proximity effect between aluminium and a lower gap superconductor, such as titanium. Titanium also features a higher kinetic inductance due to its higher penetration depth [21] leading to a significant increase of α/Δ_0^2 . However titanium was never demonstrated to work as a high quality factor resonator, possibly because of its high sensitivity to contaminants [22], yielding dissipative conducting states. This leads us naturally to protect titanium with aluminium, which is known to have an almost lossless self-protecting oxide layer. Moreover, to efficiently collect phonons from the substrate into the superconductor it is important to have an acoustic impedance matching between the substrate and the KID. In that respect, aluminium provides a better coupling to silicon than titanium [23]. The geometry, we present, is thus an Al-Ti-Al trilayer with the following thicknesses: Al 14 nm / Ti 33 nm / Al 30 nm.

The fabrication of the chip was made according to the following steps. The intrinsic 380 μm thick Si <100> wafer is dipped for 1 min in dilute 5% HF solution and then rinsed in deionized water for 1 min. The wafer is then moved to an electron beam evaporator dedicated to superconducting materials, where the layers are subsequently evaporated at rates of 0.5 nm/s in a residual vacuum of 4×10^{-8} mb. This is important especially for titanium to avoid trapping impurities in the layer [22]. The film is patterned using standard UV lithography followed by a two-steps wet etching. In a first step, the aluminium is removed using a commercial acids mixture solution. Then, in the second step, the titanium and the bottom aluminium layers are softly etched in diluted HF (0.05%).

The sensor implements a LEKID design [24] identical to the Al detector in [19]. Its active area consists of an inductive meander made of 30 connected strips of $62.5 \mu\text{m} \times 2 \text{ mm}$. The meander is closed with a capacitor made of 2 interdigitated fingers of $1.2 \text{ mm} \times 50 \mu\text{m}$. The silicon substrate is cut into a $2 \times 2 \text{ cm}^2$ detector with the KID in the center as shown in Figure 1. The chip is assembled in a copper structure

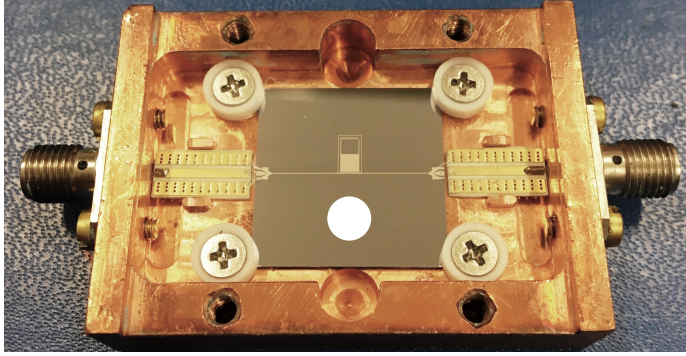


Figure 1. The detector, made by a KID deposited on a $2 \times 2 \text{ cm}^2$ silicon substrate, is assembled in a copper structure through 4 PTFE supports. The circle show the position and size of the spot of the optical system used to illuminate the substrate.

through 4 PTFE supports with total contact area of about 3 mm^2 . The copper holder is thermally anchored to the coldest point of a $^3\text{He}/^4\text{He}$ dilution refrigerator with base temperature lower than 10 mK.

3. Electrical and thermal characterization of the detector

The electrical characterization of the KID is based on the study of the complex transmission (S_{21}) of the resonator around the resonant frequency (Figure 2). The frequency dependence of the transmission of a resonator is ideally well described by a single-pole approximation. It is however necessary to take into account also impedance mismatches, power distortion and electronics non-linearity to perform a rigorous estimation [25]. This measurement allows one to extract the coupling quality factor Q_c , the internal quality factor Q_i and the total quality factor $Q = (Q_c^{-1} + Q_i^{-1})^{-1}$.

The resonant frequency is found to be close to 2.4 GHz. Q_c is 1.48×10^5 in very good agreement with the value predicted by the SONNET electromagnetic simulation of about 1.5×10^5 . Q_i is estimated as 6×10^5 , lower than our typical samples made of aluminium [19], but high enough to allow the good operation of the detector.

The critical temperature and the resistance of the trilayer film have been measured in a 4-terminal geometry. The superconducting transition was measured at $(805 \pm 10) \text{ mK}$ with a normal state resistance per square $R_{sq} = 0.58 \text{ } \Omega/\text{sq}$ above the transition. We estimate theoretically the T_C of the trilayer following [26], assuming perfect interface transparency to phonons across the layers and a superconductor thickness comparable to its coherence length. Solving the Usadel equations [27] within these assumptions yields an analytical dependence of T_C on the thickness of the layers, similar to what found in the Cooper model [28]. To apply straightforwardly this bilayer model to the Al/Ti/Al trilayer, we treat it as

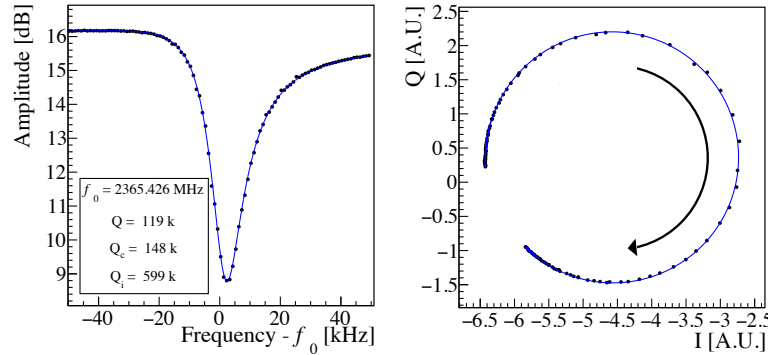


Figure 2. Complex transmission coefficient (S_{21}) around resonance compared to fit (blue line). Left: $|S_{21}|$ vs frequency. Right: Same data in the complex IQ plane. The arrow indicates the direction of increasing frequency.

a bilayer Al-Ti taking the average thicknesses of the Al layers [29]. The expected critical temperature from this model is $T_C = 720$ mK, assuming values of T_C for the single layers that take into account the increase of critical temperature in thin films, as described in [30]. The discrepancy between the expected T_C and the measured value may come from the limitations of the model: we miss the precise values of the electron-phonon coupling in all the layers, the actual transparency of the interfaces and also the actual T_C for each layer. A systematic study of those will be the subject of a separated work.

Using the SONNET electromagnetic simulations software we estimate the amount of kinetic inductance L_k needed to shift the resonant frequency from the value simulated for a perfect conductor ($L_K = 0$) to the measured value. We obtain a value of 1.4 pH/sq, that is significantly higher than the value of 1.0 pH/sq obtained using the BCS form described in [14], that depends on T_C and R_{sq} . This is a first hint, that our case of inhomogeneous superconductor can not be well described by the BCS theory. The obtained value of kinetic inductance translates into a kinetic inductance fraction $\alpha=17\%$, much larger than the ones obtained in aluminium ($\alpha=2.5\%$) using the same design [19].

We have also measured the relative variations of the resonant frequency $(f - f_0)/f_0$ as a function of the temperature (Figure 3). These data are compared with a model developed by Gao *et al.*[31] using the Mattis-Bardeen theory. The model is calculated for our best estimation of the parameters ($T_C = 805$ mK and $\alpha = 17\%$). Again the BCS form cannot describe properly the case of our inhomogeneous superconductor and we can indeed see the data departing from the BCS model at intermediate temperatures. The interpretation of these measurements needs a dedicated model, whose development is beyond the scope of this paper. However it has to be stressed that high Q resonators can be used to investigate several properties of non-standard superconductors.

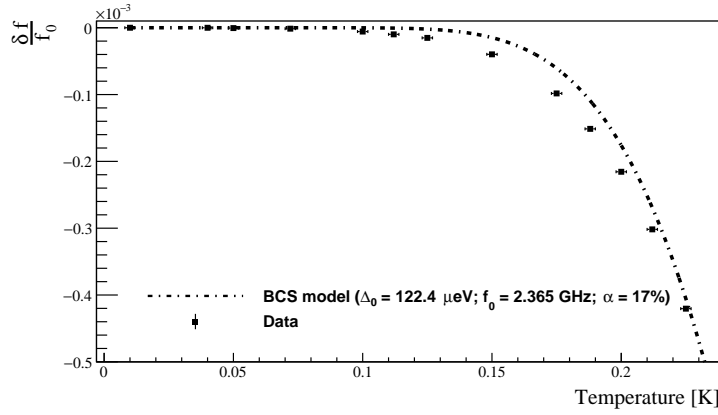


Figure 3. Measured relative variations of the resonant frequency $(f - f_0)/f_0$ as a function of temperature (black squares), compared to the Mattis-Bardeen theory (dashed lines)

4. Detector performance

Our experimental setup allows to back-illuminate the detector using two different sources: a non-collimated X-ray ^{55}Fe source and an optical fiber coupled to a fast room-temperature LED. The ^{55}Fe source illuminates in an almost uniform way the whole substrate with a rate of 1 Hz. The LED emits photons at 400 nm in the typical range of Cherenkov light. Depending on the LED pulse duration and/or amplitude, a variable number of photons can be sent onto the substrate. The whole optical system is initially calibrated with an accuracy of 10 % using a PMT at room temperature and then cross-calibrated with the ^{55}Fe source. The position and size of the optical system spot on the substrate is shown in Figure 1.

The resonator is excited and probed with a monochromatic tone at the resonant frequency f_0 . The output signal is fed into a CITLF3 SiGe cryogenic low noise amplifier, downconverted at room temperature using a superheterodyne electronics and then digitized with an acquisition card at a sampling frequency of 500 kSPS. Time traces of up to 12 ms of the real (I) and imaginary (Q) parts of S_{21} are acquired following a software trigger. Finally I and Q variations are converted into changes of phase and amplitude relative to the center of the resonance loop. A detailed description of the experimental setup of our laboratory at INFN Rome, including the room-temperature electronics and the acquisition software, can be found in references [7, 32].

As already mentioned, the phase response is typically larger than the amplitude one. However the phase noise exhibits often an excess noise, which sometimes makes it advantageous to consider both phase and amplitude responses in the analysis of the detector sensitivity. When amplitude and phase noises are dominated by the noise of the low noise amplifier, they decrease with microwave power as $S_\varphi \propto P_{\text{in}}^{-1/2}$; however at large powers the non-linearities of the kinetic inductance

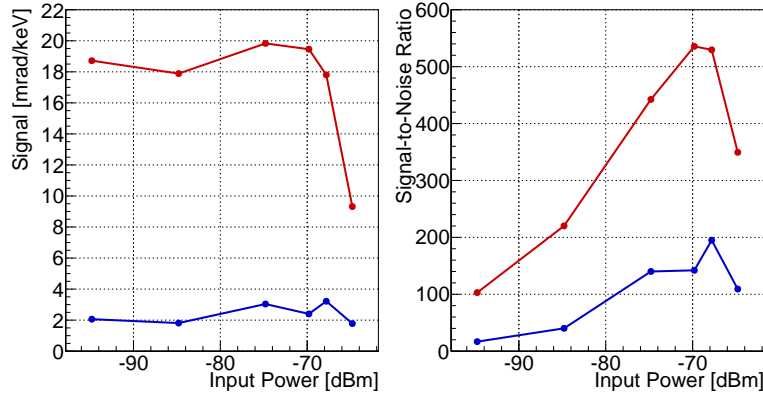


Figure 4. Results of the power scan, obtained by sending light pulses of 15.5 keV on the detector. Left: Phase (red) and amplitude (blue) signal height in mrad as function of the bias power. Right: Signal-to-Noise ratio as function of bias power. The optimal working point is chosen sat -70 dBm.

and heating effects become relevant [33]: the increase of the QP's density provokes losses that suppress the signal. The recombination time τ_{QP} , which determines the signal integration time [34], is also reduced, lowering the signal-to-noise ratio. For these reasons, it is important to determine experimentally the bias power leading to the optimal signal-to-noise ratio.

For this purpose, we perform a microwave power scan from about -95 dBm to -65 dBm at the input of the sample, while the monitoring signal and noise levels, as well as the pulse shape, in both the phase and amplitude readouts. A reference signal is produced by sending light pulses of 15.5 keV. The signals are processed using a matched filter, a software algorithm that allows to improve the signal-to-noise ratio by suppressing the signal frequencies that are mostly affected by noise [35]. The height of the filtered pulses is reported in Figure 4 left. The phase response is quite flat with increasing power around 19 mrad/keV, a sizeable improvement with respect to the 6 mrad/keV obtained with the Al detector in [19]. A similar increase is observed for the amplitude response, around 2.5 mrad/keV with respect to the 0.6 mrad/keV obtained with the Al detector.

In Figure 4 right we show the signal-to-noise ratio, obtained by dividing the amplitude of the pulses by the RMS of their baseline (after the matched filter). We determine an optimal working power of -70 dBm, about 10 dB lower than what obtained with aluminium. This behavior can be ascribed to higher non-linearities due to the higher kinetic inductance of the trilayer, as well as to the losses that could be produced by possible subgap excitations in the states spectrum of the superconductor.

The trailing edge of the pulse is well described by a single exponential law with a decay time that varies between $800 \mu\text{s}$ and $100 \mu\text{s}$ with increasing microwave power (Figure 5). As shown in [34], this decay constant can be interpreted as τ_{QP} .

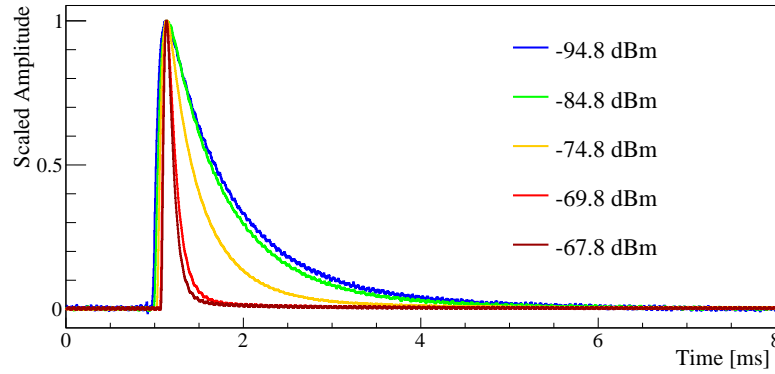


Figure 5. Response of the resonator to light pulses of 15.5 keV for increasing microwave powers. The time traces are obtained by averaging many waveform to reduce the random noise and their amplitude is normalized to 1 to highlight the shape variation.

The noise power spectrum at optimal power is reported in Figure 6 for both the phase and amplitude readouts. The flat noise observed in the amplitude readout and in the high frequency region of the phase readout, is consistent with the noise temperature of the cold amplifier ($T_N \sim 6 K$). This noise is exceeded by a low-frequency phase noise, whose spectral index is found to be 0.49 ± 0.05 , consistent with the presence of a two-level system noise in the detector, observed often in KIDs [36]. Both power spectra show also peaks due to the readout electronics. These peaks do not affect significantly the energy resolution, since they are strongly suppressed by the matched filter.

To obtain a solid estimation of the detector performance we implement a calibration based on the Poisson statistics of the photons absorbed into the substrate. The detector is biased at the optimal microwave power of -70 dBm and is illuminated with optical pulses of energies in the range 0 - 3 keV. For each energy the distribution

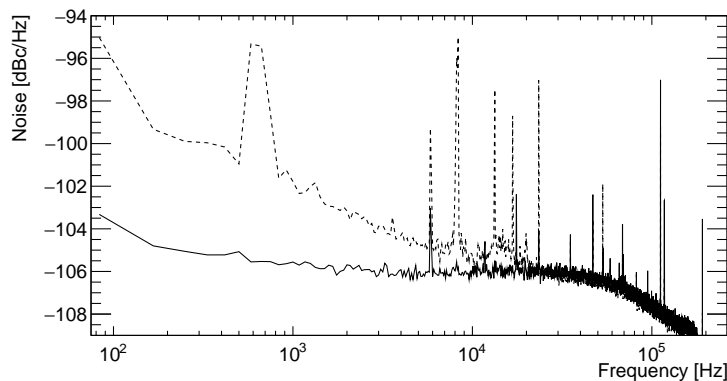


Figure 6. Average noise power spectrum in phase (dotted line) and amplitude (solid line) readouts. More details in the text.

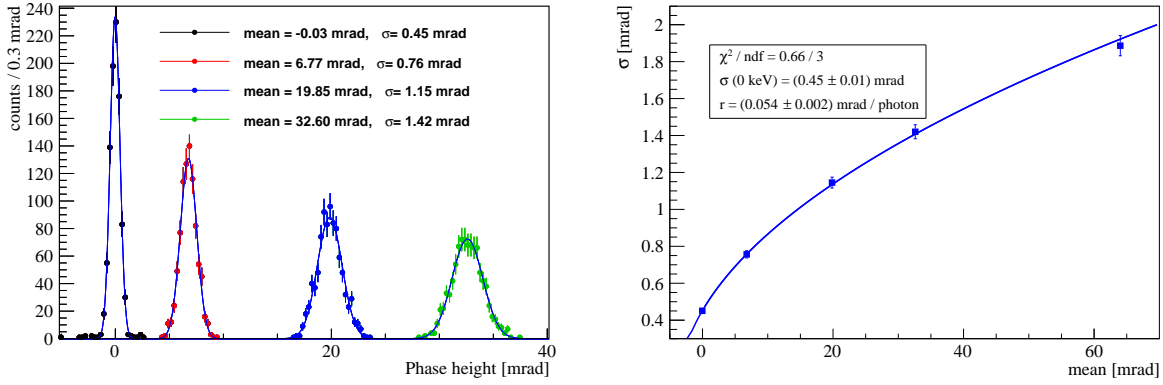


Figure 7. Left: Histograms of pulse heights in the phase readout for light signals of different energies. Right: Standard deviation σ versus mean m of the Gaussian distributions shown in the left panel. The plot includes one more point at 65 mrad not shown in the left panel to not compress the scale for the other distributions. The curve is well described by the Poisson statistics of photons. See the text for more details.

of the pulse heights in the phase readout is found to be well described by a Gaussian with mean m and standard deviation σ (Figure 7 left). The σ vs m data are then fitted (Figure 7 right) assuming that two uncorrelated components contribute to the detector resolution: the baseline resolution (σ_0) and the Poissonian term from the photon counting that we model as $\sqrt{m \times r}$, where r is the responsivity per photon: $\sigma = \sqrt{\sigma_0^2 + m \times r}$. The responsivity in energy can be found by dividing r by the energy of a single 400 nm photon. We find a responsivity of $(17.54 \pm 0.58 \text{ mrad/keV})$ in good agreement with the calibration against ^{55}Fe presented previously in this Section. Using this energy calibration we find a phase readout baseline resolution $\sigma_\phi = (25.64 \pm 0.85) \text{ eV}$. Applying the same procedure to the amplitude readout, we obtain $\sigma_A = (77.3 \pm 2.5) \text{ eV}$.

5. Conclusions and discussions

In this paper we presented the results obtained using an Al/Ti/Al trilayer film to develop a phonon-mediated KID for the detection of UV-VIS light on large surfaces. The sample features $T_C = 805 \text{ mK}$, $Q_i \simeq 600 \text{ k}$ and a low-power recombination time $\tau_{QP} = 800 \mu\text{s}$. The main features of the detector are compared in Table 1 with the Al detector, presented in [19]. The lower critical temperature allows us to increase significantly the fraction of kinetic inductance α and consequently the responsivity of the detector. The overall result is the improvement of the RMS baseline resolution for phase readout from 105 eV down to 26 eV.

This result approaches the target resolution of the CALDER project of 20 eV. The last phase of the project - currently in progress - consists in the development of light detectors of $5 \times 5 \text{ cm}^2$.

	Al KID	Al/Ti/Al KID
T_c [mK]	1.18	0.805
Q_i [k]	> 2000	600
α	0.025	0.17
Phase resp. [mrad/keV]	5.8	17.6
Amplitude resp. [mrad/keV]	0.6	2.5
σ_A [eV]	115	77
σ_ϕ [eV]	105	26
σ_T [eV]	82	26

Table 1. Main features of the detector presented in this paper compared with the Al detector described in [19]. σ_T is the resolution obtained for the combination of phase and amplitude readout, using a 2D matched filter [19].

Acknowledgements

This work was supported by the European Research Council (FP7/2007-2013) under contract CALDER no. 335359 and by the MIUR under the FIRB contract no. RBFR1269SL. The authors thanks the personnel of INFN Sezione di Roma for the technical support, in particular M. Iannone, F. Pellegrino, L. Recchia and D. Ruggeri. HLS,MC, JG and AM acknowledge support from the ANR grant ELODIS2 no. ANR-16-CE30-0019-02.

- [1] Day P K, LeDuc H G, Mazin H G, Vayonakis A and Zmuidzinas J 2003 *Nature* **425** 817
- [2] Monfardini A et al 2011 *Astrophys.J.Suppl.* **194**
- [3] Mazin B et al 2013 *Pub. of the Astronomical Society of the Pacific* **125** 1348
- [4] Cook T et al 2015 *J. Astron. Telescopes, Instruments, and Systems* **1** id. 044001
- [5] Quaranta O, Cecil T W, Gades L, Mazin B and Miceli A 2013 *Sup. Sci. Tech.* **26** 105021
- [6] Faverzani M et al 2014 *J. Low. Temp. Phys.* **176** 530
- [7] Battistelli E S et al 2015 *EPJ C* **75** 353
- [8] Artusa D R et al 2015 *Adv. High En. Phys.* **2015** 879871
- [9] Tabarelli de Fatis T 2010 *Eur. Phys. J. C* **65** 359
- [10] Casali N et al 2015 *Eur. Phys. J. C* **75** 12
- [11] Casali N 2017 *Astropart. Phys.* **91** 44
- [12] Wang G et al 2015 arXiv:1504.03599 [physics.ins-det]
- [13] Artusa D R et al 2014 *Eur. Phys. J. C* **74** 3096
- [14] Zmuidzinas J 2012 *Annual Review of Condensed Matter Physics* **3** 169
- [15] Swenson L J, Cruciani A, Benoit A, Roesch M, Yung C S, Bideaud A and Monfardini A 2010 *Appl.Phys.Lett.* **96** 263511
- [16] Cruciani A, Swenson L J, Monfardini A, Boudou N, Calvo M and Roesch M 2012 *J. Low Temp. Phys.* **167** 311
- [17] Moore D C, Golwala S R, Bumble B, Cornell B, Day P K, LeDuc H G and Zmuidzinas J 2012 *Appl. Phys. Lett.* **100**, 262601,
- [18] Cardani L et al 2015 *Appl.Phys.Lett.* **107** 093508
- [19] Cardani L et al 2017 *Appl. Phys. Lett.* **110** 033504
- [20] Gao J, Zmuidzinas J, Vayonakis A, Day P, Mazin B, and Leduc H 2008 *J. Low Temp. Phys.* **151** 557
- [21] Tinkham M, 2004 *Introduction to Superconductivity*

- [22] Peruzzi A, Gottardi E, Peroni I, Ponti G and Ventura G 1999 *Nucl. Phys. B* **78** 576
- [23] Kaplan S B 1979 *J. Low Temp. Phys.* **37** 343
- [24] Doyle S, Naylon J, Mauskopf P D, Porch A and Dunscombe C 2008 *J. Low Temp. Phys.* **151** 530
- [25] Casali N et al 2016 *J. Low Temp. Phys.* **184** 142
- [26] Catalano A et al 2015 *Astron. Astrophys* **580** A15
- [27] Usadel K D 1970 *Phys. Rev. Lett.* **25** 570
- [28] Cooper L N 1961 *Phys. Rev. Lett.* **6** 689
- [29] Le Suer H, PhD Thesis, Universite Paris 6 (2007)
- [30] Strongin M, Kammerer O F and Paskin A 1965 *Phys. Rev. Lett.* **14** 949
- [31] Gao J 2006 *NIMPA* **559** 585
- [32] Bourrion O , Bideaud A, Benoit A, Cruciani A, Macias-Perez J F, Monfardini A, Roesch M, Swenson L J and Vescovi C 2011 *JINST* **6** P06012
- [33] Goldie D J, Withington S 2013 *Supercond. Sci. Technol.* **26** 1
- [34] Cruciani A et al 2016 *J. Low Temp. Phys.* **184** 859
- [35] Gatti E, Manfredi P F 1986 *Riv. Nuovo Cimento* **9** 1
- [36] Gao J, Daal M, Vajonakis A, Kumar S, Zmuidzinas J, Sadoulet B, Mazin B A, Day Pk, Leduc H G 2008 *Appl. Phys. Lett.* **92** 152505